Chapter 1
Classical Scattering Theory

1.1 Relative Motion of Projectile and Target

Consider two particles, projectile and target, with masses m_1 and m_2 respectively, which interact via a time-independent potential V depending on the separation

$$\mathbf{r} = \mathbf{r}_1 - \mathbf{r}_2 \tag{1.1}$$

of their position vectors $\mathbf{r}_1$ and $\mathbf{r}_2$. In the absence of external forces, the centre of mass $\mathbf{R}_{\rm cm} = (m_1\mathbf{r}_1 + m_2\mathbf{r}_2)/(m_1 + m_2)$ moves uniformly, $\mathbf{R}_{\rm cm}(t) = \mathbf{R}_{\rm cm}(0) + \mathbf{V}_{\rm cm}t$. In the *centre-of-mass frame of reference*, that is the inertial system in which the centre of mass of the two particles is at rest, the position vectors of the two particles are

$$\mathbf{r}_1^{(\rm cm)} = \frac{m_2}{m_1 + m_2}\mathbf{r}, \qquad \mathbf{r}_2^{(\rm cm)} = -\frac{m_1}{m_1 + m_2}\mathbf{r}. \tag{1.2}$$

Scattering experiments in the laboratory usually involve a projectile initially moving freely towards a target at rest,

$$\mathbf{r}_1^{(\rm in,\,lab)}(t) = \mathbf{r}_1^{(\rm in,\,lab)}(0) + \mathbf{v}_1^{(\rm in,\,lab)}t, \qquad \mathbf{r}_2^{(\rm in,\,lab)}(t) = \mathbf{r}_2^{(\rm in,\,lab)}(0), \tag{1.3}$$

so the centre-of-mass velocity in the *laboratory frame of reference* is simply $\mathbf{V}_{\rm cm}^{(\rm lab)} = \dot{\mathbf{r}}_1^{(\rm in,\,lab)} m_1/(m_1 + m_2)$.

Throughout this book we shall focus on the *relative motion* of projectile and target, which contains the essential nontrivial physics of the scattering problem. The relevant coordinate is the relative distance (1.1). Transformation to the laboratory frame of reference is achieved via (1.2) and $\mathbf{r}_i^{(\rm lab)}(t) = \mathbf{r}_i^{(\rm cm)}(t) + \mathbf{R}_{\rm cm}^{(\rm lab)}(t)$, $i = 1, 2$. Details of such straightforward but cumbersome transformations are discussed, e.g., in paragraph 17 of [2].

Classically, the evolution of $\mathbf{r}(t)$ is described by Newton's equation of motion

$$\mu\ddot{\mathbf{r}} = -\nabla V(\mathbf{r}), \quad \mu = \frac{m_1 m_2}{m_1 + m_2}, \tag{1.4}$$

as for one particle with the *reduced mass* μ moving under the influence of the potential $V(\mathbf{r})$. In accordance with standard convention, we assume the asymptotic incoming velocity $\mathbf{v}_\infty = \lim_{t\to-\infty}\dot{\mathbf{r}}(t)$ to point in the direction of the positive z-axis,

H. Friedrich, *Scattering Theory*, DOI 10.1007/978-3-662-48526-2_1

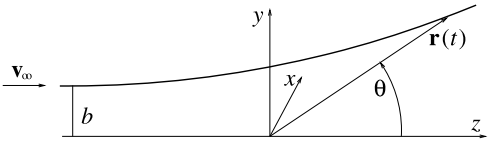

Fig. 1.1 Scattering of a particle with asymptotic incoming velocity $\mathbf{v}_\infty$

as illustrated in Fig. 1.1. We assume the potential $V(\mathbf{r})$ to vanish asymptotically, so the conserved total energy E of the system is just the incoming particle's initial kinetic energy, $E = \frac{1}{2}\mu v_\infty^2$, where $v_\infty = |\mathbf{v}_\infty|$. The perpendicular displacement of the incoming particle's asymptotic straight-line trajectory from the z-axis is the *impact parameter* b, so the incoming particle has an initial angular momentum $|\mathbf{L}| = \mu b v_\infty$ around the origin.

1.2 Deflection Function

From now on we assume that the potential $V(\mathbf{r})$ is radially symmetric; it depends only on the modulus r of the distance vector $\mathbf{r}$ and not on its orientation. The angular momentum $\mathbf{L} = \mu \mathbf{r} \times \dot{\mathbf{r}}$ is thus a conserved vector which always points in the same direction, and both $\mathbf{r}$ and $\dot{\mathbf{r}}$ must lie in the plane perpendicular to this direction. Any trajectory $\mathbf{r}(t)$ describing the scattering of the particle by the potential $V(r)$ is confined to a plane, the *scattering plane*. As already anticipated in Fig. 1.1, we choose it to be the y–z plane, and we assume that the positive x-axis points in the direction of $\mathbf{L}$, so $L = |\mathbf{L}| = L_x \geq 0$.

For motion in the y–z plane, the polar coordinates r, θ are defined via

$$x \equiv 0, \qquad y = r \sin\theta, \qquad z = r \cos\theta, \tag{1.5}$$

and the (conserved) angular momentum is

$$L = L_x = \mu(y\dot{z} - z\dot{y}) = -\mu r^2 \dot{\theta} = \mu b v_\infty. \tag{1.6}$$

Since the conserved energy is $E = \frac{1}{2}\mu v_\infty^2$, the impact parameter b is related to the angular momentum L and energy E via

$$L = b\sqrt{2\mu E}. \tag{1.7}$$

According to the geometry of Fig. 1.1, b and L are nonnegative, so

$$\dot{\theta} = -\frac{L}{\mu r^2} \leq 0, \tag{1.8}$$

which, for given L, uniquely defines $\dot{\theta}$ as function of r and shows that $\theta(t)$ is a monotonically decreasing function in time, starting from its initial value $\theta(t) \overset{t \to -\infty}{=} \pi$.

After the particle is scattered by the potential, it leaves to large r and its trajectory approaches a straight line deflected by the angle Θ from the forward direction. The deflection angle Θ depends on the energy E and the impact parameter b. For a given

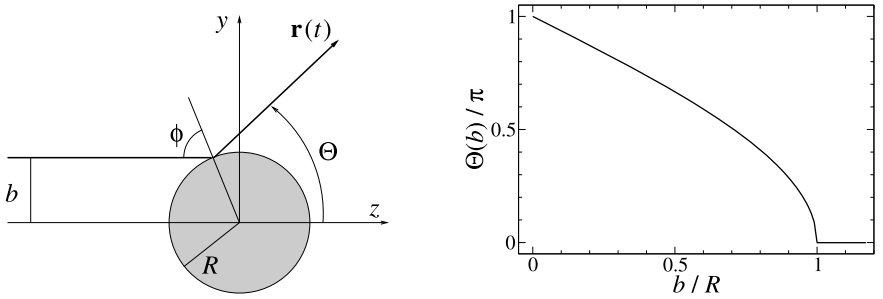

Fig. 1.2 Scattering by a hard sphere of radius R. Deflection function (1.9)

scattering experiment, the energy can be taken as fixed and known, so the observable features are determined by the function $\Theta(b)$, which is called the *deflection function*. We write the capital letter and emphasize that Θ retains the memory of possible clockwise revolutions around the scattering centre.

One of the simplest conceivable scattering problems is the scattering by a hard sphere of radius R as illustrated in the left-hand part of Fig. 1.2. The deflection angle is $\pi - 2\phi$, where $\sin\phi = b/R$,

$$\Theta(b) = \pi - 2\arcsin\left(\frac{b}{R}\right) = 2\arccos\left(\frac{b}{R}\right) \quad \text{for } 0 \le b \le R. \tag{1.9}$$

Obviously, trajectories with $b > R$ are not deflected, $\Theta(b) = 0$ for $b > R$. The deflection function (1.9) is shown in the right-hand part of Fig. 1.2.

More realistic scattering problems involve a smooth potential $V(r)$, for which the scattering trajectory cannot be constructed by such simple geometric means. In polar coordinates we have $E = \frac{1}{2}\mu(\dot{r}^2 + r^2\dot{\theta}^2) + V(r)$; with (1.8):

$$E = \frac{\mu}{2}\dot{r}^2 + \frac{L^2}{2\mu r^2} + V(r). \tag{1.10}$$

Equation (1.10) is a one-dimensional energy-conservation formula for the radial motion described by the coordinate r and the velocity $\dot{r}$. It shows that the evolution of $r(t)$ is as for one-dimensional motion of a particle with mass μ on the half-line $r \ge 0$ under the influence of an *effective potential*, V_{eff}. The effective potential consists of the potential energy $V(r)$ and the *centrifugal potential* $V_{\text{cent}}(r)$, which comes from the kinetic energy of angular motion and depends on the angular momentum L,

$$V_{\text{eff}}(r) = V(r) + V_{\text{cent}}(r), \quad V_{\text{cent}}(r) = \frac{L^2}{2\mu r^2}. \tag{1.11}$$

The effective potential helps us to understand the behaviour of a scattering trajectory for given energy E and impact parameter b (or angular momentum $L = b\sqrt{2\mu E}$) in very straightforward terms. The scattering process begins with $r \to \infty$ for $t \to -\infty$, and r decreases with time until it reaches the *classical turning point* r_{ctp}, which fulfills

$$E = V_{\text{eff}}(r_{\text{ctp}}) \tag{1.12}$$

and corresponds to the point of closest approach of target and projectile. For the hard-sphere case in Fig. 1.2, $r_{\rm ctp}$ is the sphere's radius R as long as $b \le R$. If $V_{\rm eff}(r) < E$ for all r, then the radial turning point is the origin, $r_{\rm ctp} = 0$. It is a useful convention to choose the time of closest approach to be $t = 0$: $r(t = 0) = r_{\rm ctp}$. For later (positive) times, r increases again until $r \to \infty$ for $t \to +\infty$.

The trajectory of the particle in the y–z-plane is most conveniently obtained via $\mathrm{d}\theta/\mathrm{d}r = \dot\theta/\dot r$ with $\dot\theta$ from (1.8) and $\dot r = \pm\sqrt{(2/\mu)[E - V_{\rm eff}(r)]}$ from (1.10),

$$\frac{\mathrm{d}\theta}{\mathrm{d}r} = \pm\frac{L}{r^2\sqrt{2\mu[E - V_{\rm eff}(r)]}}. \tag{1.13}$$

During the first half of the scattering process, $\dot r$ is negative (as is $\dot\theta$), so the plus sign on the right-hand side of (1.13) applies. During the second half, $\dot r$ is positive (in contrast to $\dot\theta$), so (1.13) applies with the minus sign. The polar angle of the point of closest approach, for which $r = r_{\rm ctp}$, is

$$\theta(r = r_{\rm ctp}) = \pi + \int_{\infty}^{r_{\rm ctp}} \frac{\mathrm{d}\theta}{\mathrm{d}r}\mathrm{d}r = \pi - \int_{r_{\rm ctp}}^{\infty} \frac{L \quad \mathrm{d}r}{r^2\sqrt{2\mu[E - V_{\rm eff}(r)]}}. \tag{1.14}$$

For an actual calculation, the scattering trajectory (r, θ) in the y–z plane can be obtained via

$$\theta(r) = \theta(r = r_{\rm ctp}) \pm \int_{r_{\rm ctp}}^{r} \frac{L \quad \mathrm{d}r'}{r'^2\sqrt{2\mu[E - V_{\rm eff}(r')]}}, \tag{1.15}$$

where the plus sign gives the points on the incoming half of the trajectory and the minus sign the points on the outgoing half. The deflection function follows from the expression (1.15) for the polar angle in the limit $r \to \infty$ on the outgoing branch of the trajectory,

$$\begin{aligned}\Theta(b) &= \theta(r_{\rm ctp}) - \int_{r_{\rm ctp}}^{\infty} \frac{L \quad \mathrm{d}r}{r^2\sqrt{2\mu[E - V_{\rm eff}(r)]}} = \pi - \int_{r_{\rm ctp}}^{\infty} \frac{2L \quad \mathrm{d}r}{r^2\sqrt{2\mu[E - V_{\rm eff}(r)]}} \\ &= \pi - \int_{r_{\rm ctp}}^{\infty} \frac{2b}{r^2}\left[1 - \frac{b^2}{r^2} - \frac{V(r)}{E}\right]^{-1/2} \mathrm{d}r. \end{aligned} \tag{1.16}$$

In the limit of large impact parameters, the effective potential (1.11) is dominated by the centrifugal term and the deflection angle tends to zero. For a potential falling off asymptotically as an inverse power of r,

$$V(r) \overset{r\to\infty}{\sim} \frac{C_\alpha}{r^\alpha}, \quad \alpha > 0, \tag{1.17}$$

the large-b behaviour of $\Theta(b)$ is easily calculated analytically. Changing the integration variable in (1.16) from r to $\xi = r/r_{\rm ctp}$ gives, for large b,

$$\Theta(b) = \pi - \int_1^{\infty} \frac{2\,\mathrm{d}\xi}{\sqrt{\xi^4 - \xi^2 + \varepsilon(\xi^4 - \xi^{4-\alpha})}}, \quad \text{where } \varepsilon = \left(\frac{r_{\rm ctp}}{b}\right)^2 - 1. \tag{1.18}$$

Expanding the integrand in terms of the small parameter $\varepsilon \overset{b\to\infty}{\sim} C_\alpha/(E\,b^\alpha)$ yields

$$\Theta(b) \overset{b\to\infty}{\sim} \frac{C_\alpha}{E\,b^\alpha}\frac{\pi\,\Gamma(\alpha)}{2^{\alpha-1}[\Gamma(\frac{\alpha}{2})]^2} = \frac{C_\alpha}{Eb^\alpha}\frac{\sqrt{\pi}\,\Gamma(\frac{\alpha+1}{2})}{\Gamma(\frac{\alpha}{2})}. \tag{1.19}$$

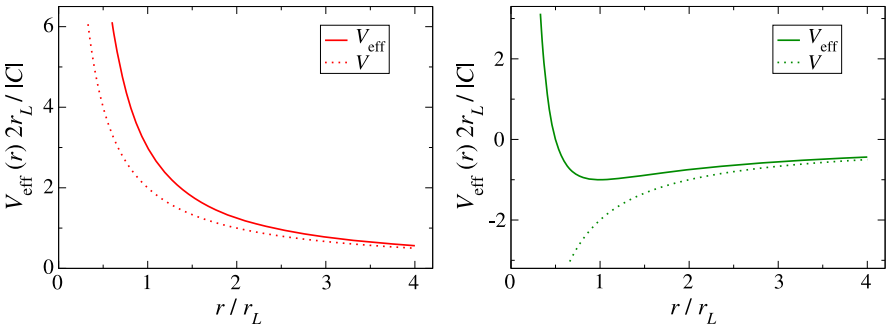

Fig. 1.3 Effective potential (1.21) for a repulsive ($C > 0$, *left-hand part*) and an attractive ($C < 0$, *right-hand part*) Kepler–Coulomb interaction. The *dotted lines* show the respective potential (1.20) without centrifugal contribution

1.2.1 Kepler–Coulomb Potential

The Kepler or Coulomb potential,

$$V(r) = \frac{C}{r}, \tag{1.20}$$

is important, because it describes gravitational and electrostatic interactions. For such a homogeneous potential of degree -1, the solutions of Newton's equation of motion (1.4) obey a simple scaling relation called Kepler's third law. If $\mathbf{r}(t)$ is a solution at energy E, then $s\mathbf{r}(s^{3/2}t)$ is a solution at energy E/s, see Appendix A.1. The geometric shape of a trajectory does not depend on the potential strength coefficient C, the impact parameter b and the energy E independently, but only on the ratio of C to the product Eb.

The weight of the centrifugal contribution in the effective potential (1.11) can be expressed via the length parameter

$$r_L = \frac{L^2}{\mu|C|}, \quad \text{so} \quad V_{\rm eff}(r) = \frac{|C|}{2r_L}\left[\pm 2\frac{r_L}{r} + \left(\frac{r_L}{r}\right)^2\right]. \tag{1.21}$$

In the repulsive case, $C > 0$, the plus sign in the square bracket applies; the effective potential is a monotonically decreasing function of r. In the attractive case, $C < 0$, $V_{\rm eff}(r)$ has a zero at $r_L/2$ and a minimum at r_L with $V_{\rm eff}(r_L) = -|C|/(2r_L)$. The effective potential (1.21) is shown for both the repulsive and the attractive case in Fig. 1.3.

The classical turning point is

$$r_{\rm ctp} = b\left(\sqrt{\gamma^2 + 1} \pm \gamma\right) \quad \text{with } \gamma = \frac{|C|}{2Eb}, \tag{1.22}$$

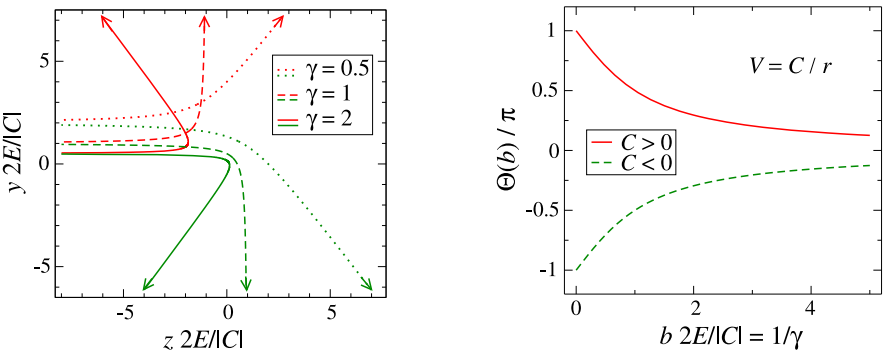

Fig. 1.4 Scattering trajectories (*left-hand part*) and deflection function *right-hand part* for the Kepler–Coulomb potential (1.20). The *red* (*green*) *lines* correspond to the repulsive (attractive) case $C > 0$ ($C < 0$). Lengths are in units of $|C|/(2E)$

where the plus (minus) sign applies for the repulsive (attractive) case $C > 0$ ($C < 0$) and the geometry of the trajectory is governed by the dimensionless parameter γ. With $\rho = r/b$, Eqs. (1.14) and (1.15) are as follows for the Kepler–Coulomb case:

$$\begin{aligned} \theta(\rho_{\mathrm{ctp}}) &= \pi - \int_{\rho_{\mathrm{ctp}}}^{\infty} \frac{\mathrm{d}\rho}{\rho\sqrt{\rho^2 \mp 2\gamma\rho - 1}}, \\ \theta(\rho) &= \theta(\rho_{\mathrm{ctp}}) \pm \int_{\rho_{\mathrm{ctp}}}^{\rho} \frac{\mathrm{d}\rho'}{\rho'\sqrt{\rho'^2 \mp 2\gamma\rho' - 1}}. \end{aligned} \tag{1.23}$$

The minus (plus) sign in the square root applies for the repulsive (attractive) case $C > 0$ ($C < 0$). Typical trajectories are shown in the left-hand part of Fig. 1.4. The axes are labelled with the b-independent dimensionless lengths $\rho\cos\theta/\gamma \equiv z2E/|C|$, $\rho\sin\theta/\gamma \equiv y2E/|C|$. The right-hand part of Fig. 1.4 shows the deflection function,

$$\Theta(b) = \pi - \int_{\rho_{\mathrm{ctp}}}^{\infty} \frac{2\,\mathrm{d}\rho}{\rho\sqrt{\rho^2 \mp 2\gamma\rho - 1}} = \pm 2\arccos\left(\frac{1}{\sqrt{\gamma^2+1}}\right). \tag{1.24}$$

1.2.2 Inverse-Power Potentials

As a more general ansatz, consider the inverse-power potential,

$$V(r) = \frac{C_\alpha}{r^\alpha}, \quad \alpha > 0. \tag{1.25}$$

This is a homogeneous potential of degree $-\alpha$, and, as a generalization of Kepler's third law, the solutions of Newton's equation of motion (1.4) obey the following scaling relation: If $\mathbf{r}(t)$ is a solution at energy E, then $s\mathbf{r}(s^{1+\alpha/2}t)$ is a solution at energy E/s^α, see Appendix A.1. The geometric shape of a trajectory does not

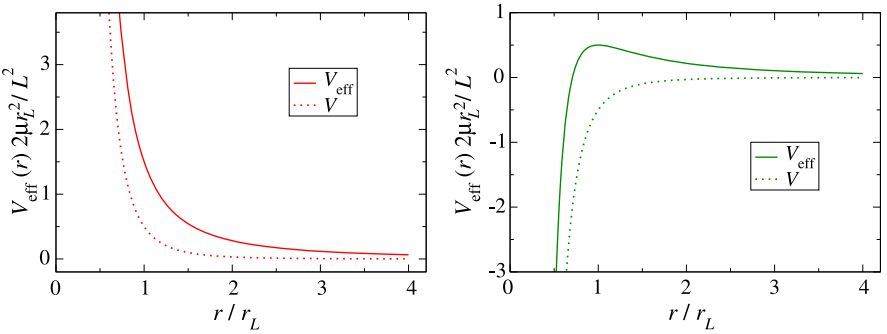

Fig. 1.5 Effective potential (1.26) for a repulsive ($C_\alpha > 0$, *left-hand part*) and an attractive ($C_\alpha < 0$, *right-hand part*) inverse-power potential with $\alpha = 4$. The *dotted lines* show the respective potential (1.25) without centrifugal contribution

depend on the potential strength coefficient C_α, the impact parameter b and the energy E independently, but only on the ratio of C_α to the product Eb^α. Although we are mainly interested in integer values of α on physical grounds, the discussion below is largely valid also for noninteger, real and positive α.

As a generalization of (1.21) we define

$$r_L = \left[\alpha\frac{\mu|C_\alpha|}{L^2}\right]^{1/(\alpha-2)}, \quad \text{so} \quad V_{\rm eff}(r) = \frac{L^2}{2\mu r_L^2}\left[\pm\frac{2}{\alpha}\left(\frac{r_L}{r}\right)^\alpha + \left(\frac{r_L}{r}\right)^2\right]. \quad (1.26)$$

For $C_\alpha > 0$, the plus sign in the square bracket applies; the effective potential is a monotonically decreasing function of r. For $C_\alpha = -|C_\alpha| < 0$, the minus sign applies, $V_{\rm eff}(r)$ has a zero at $r_L(2/\alpha)^{1/(\alpha-2)}$ and an extremum at r_L. For $\alpha < 2$ this extremum is a minimum, as in Sect. 1.2.1. For $\alpha > 2$, the extremum is a maximum. Such a "centrifugal barrier" is a characteristic property of all potentials with attractive tails falling off faster than $-1/r^2$. For the inverse-power tail (1.25) with $C_\alpha < 0$, the centrifugal barrier has its maximum at r_L and the barrier height is $V_{\rm eff}(r_L) = [1 - 2/\alpha]L^2/(2\mu r_L^2) > 0$. The effective potential (1.26) is shown for $\alpha = 4$, both for the repulsive and for the attractive case in Fig. 1.5.

Using (1.7), the equation defining turning points of the effective potential (1.26) can be written as

$$1 - \left(\frac{b}{r_{\rm ctp}}\right)^2 = \pm\frac{2}{\alpha}\gamma\left(\frac{b}{r_{\rm ctp}}\right)^\alpha \quad \text{with } \gamma = \frac{\alpha}{2}\frac{|C_\alpha|}{Eb^\alpha}. \quad (1.27)$$

In the repulsive case [plus sign in (1.27)], there is always one real solution for $r_{\rm ctp}$. In the attractive case, Eq. (1.27) always has one real solution for $r_{\rm ctp}$ if $\alpha < 2$.

For an attractive potential with $\alpha > 2$, Eq. (1.27) has no real solutions for large γ and two real solutions for small γ. For the value $\gamma_{\rm orb}$ separating these two regimes, the total energy E is exactly equal to the height $V_{\rm eff}(r_L)$ of the centrifugal barrier

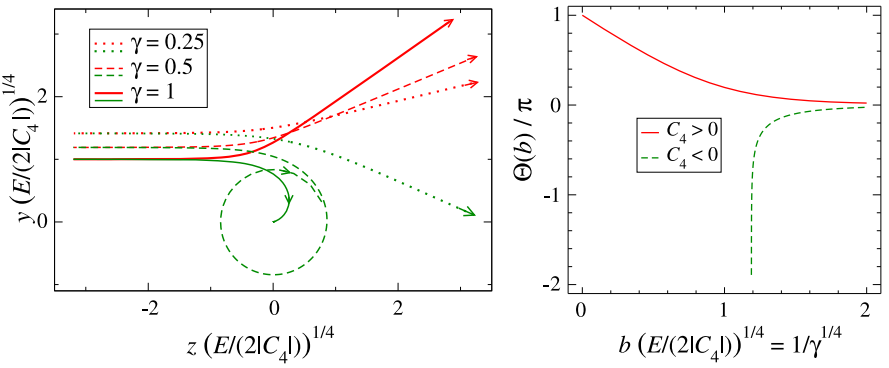

Fig. 1.6 Scattering trajectories (*left-hand part*) and deflection function (*right-hand part*) for the inverse-power potential (1.25) with $\alpha = 4$. The *red* (*green*) *lines* correspond to the repulsive (attractive) case $C_4 > 0$ ($C_4 < 0$). Lengths are in units of $(2|C_4|/E)^{1/4}$

and $r_{\rm ctp}$ is a double root of the equation; explicitly we have

$$\gamma_{\rm orb} = \left(1 - \frac{2}{\alpha}\right)^{(\alpha-2)/2} . \tag{1.28}$$

When $\gamma = \gamma_{\rm orb}$, the turning point is $r_{\rm ctp} = r_L = b\gamma_{\rm orb}^{1/(\alpha-2)}$ and Newton's equations (1.4) are solved by $\dot{r} = 0$, $\dot{\theta} = \text{const.}$ corresponding to uniform clockwise rotation on a circle of radius r_L. This motion is called *orbiting*. For fixed values of $|C_\alpha|$ and L, we have $\gamma \propto E^{(\alpha-2)/2}$, so $\gamma < \gamma_{\rm orb}$ corresponds to energies below the centrifugal barrier, where the radial motion is reflected at the outer turning point. For energies above the centrifugal barrier ($\gamma > \gamma_{\rm orb}$), there is no classical turning point and the incoming particle crashes into the origin $r = 0$ with ever increasing radial velocity. For the near-origin behaviour of the trajectory, Eq. (1.13) shows that

$$\frac{{\rm d}\theta}{{\rm d}r} \overset{r\to 0}{\sim} \frac{L}{\sqrt{2\mu|C_\alpha|}} r^{(\alpha-4)/2} \Rightarrow \int_{r_0}^{r} \frac{{\rm d}\theta}{{\rm d}r}{\rm d}r \overset{r\to 0}{\sim} c_1 - c_2 r^{(\alpha-2)/2}, \tag{1.29}$$

for a given r_0 with appropriate constants $c_{1,2}$. Since $(\alpha - 2)/2 > 0$, the polar angle converges to a finite limit during the crash to the origin.

Typical scattering trajectories are shown in the left-hand part of Fig. 1.6 for the inverse-power potential (1.25) with $\alpha = 4$. In this case $\gamma = 2|C_4|/(Eb^4)$. For $\gamma = \gamma_{\rm orb} = \frac{1}{2}$ and $C_4 < 0$, the incoming trajectory approaches the circular orbit for $t \to +\infty$. For smaller impact parameters, $\gamma > \gamma_{\rm orb}$, the incoming trajectory crashes into the origin and an outgoing trajectory cannot be determined unambiguously without further assumptions. The deflection function $\Theta(b)$ is shown in the right-hand part of Fig. 1.6. The abscissa is labelled with b in units of the length $(2|C_4|/E)^{1/4}$, i.e. with $1/\gamma^{1/4}$. For $C_4 > 0$, $\Theta(b)$ decreases monotonically from $\Theta(0) = \pi$ to zero; for $C_4 < 0$, $\Theta(b)$ increases monotonically from $-\infty$ in the orbiting case to zero. According to (1.19), $\Theta(b) \overset{b\to\infty}{\sim} \pm 3\pi\gamma/8$.

Scattering by attractive inverse-power potentials (1.25) depends crucially on whether the power α is larger or smaller than two, i.e. if there is a centrifugal barrier or not. The boundary separating these two regimes is provided by inverse-square potentials

$$V(r) = \frac{C_2}{r^2}, \qquad V_{\text{eff}}(r) = \frac{\tilde{L}^2}{2\mu r^2}, \quad \tilde{L}^2 = L^2 + 2\mu C_2. \tag{1.30}$$

As long as $\tilde{L}^2$ is greater than zero, the deflection function can be calculated in a very straightforward way. Since $\Theta(b)$ is identically zero for a free particle, the integral on the far right of the upper line of Eq. (1.16) must be equal to π for the free-particle case. This also holds for the effective potential (1.30), if we replace the true angular momentum L in the numerator of the integrand by $\tilde{L} = \sqrt{\tilde{L}^2}$, so

$$\Theta(b) = \pi\left(1 - \frac{L}{\tilde{L}}\right). \tag{1.31}$$

If $\tilde{L}^2 \leq 0$, the effective potential (1.30) has no turning point and the scattering trajectory crashes into the origin. For $\tilde{L}^2 < 0$, $\mathrm{d}\theta/\mathrm{d}r \overset{r\to 0}{\propto} 1/r$ according to (1.29), whereas $\mathrm{d}\theta/\mathrm{d}r \overset{r\to 0}{\propto} 1/r^2$ for $\tilde{L}^2 = 0$; in both cases the particle encircles the origin infinitely many times during the crash.

1.2.3 Lennard–Jones Potential

Realistic potentials have more structure than the inverse-power potentials discussed above. For example, the interaction of two neutral atoms with each other is characterized at large distances by an attractive tail proportional to $-1/r^6$, and it is strongly repulsive at very short distances comparable to the size of the atoms. A popular model for describing interatomic interactions is the Lennard–Jones potential,

$$V_{\text{LJ}}(r) = \frac{C_{12}}{r^{12}} - \frac{C_6}{r^6} = \mathscr{E}\left[\left(\frac{r_{\min}}{r}\right)^{12} - 2\left(\frac{r_{\min}}{r}\right)^{6}\right]. \tag{1.32}$$

It has a minimum at $r_{\min} = (2C_{12}/C_6)^{1/6}$, and $V_{\text{LJ}}(r_{\min}) = -\mathscr{E} = -{C_6}^2/(4C_{12})$.

We express the angular momentum in terms of a dimensionless quantity Λ,

$$\Lambda = \frac{L}{r_{\min}\sqrt{2\mu\mathscr{E}}}, \quad \text{so} \quad V_{\text{eff}} = \mathscr{E}\left[\left(\frac{r_{\min}}{r}\right)^{12} - 2\left(\frac{r_{\min}}{r}\right)^{6} + \Lambda^2\left(\frac{r_{\min}}{r}\right)^{2}\right]. \tag{1.33}$$

Λ^2 is the ratio of the centrifugal potential at $r_{\min}$ to the depth $\mathscr{E}$ of the potential (1.32). Figure 1.7 shows the effective potential (1.33) for $\Lambda^2 = 0, 1, 2$ and 3. Note that $V_{\text{eff}}(r)$ only has a local maximum if the angular momentum is less than a limiting value, $\Lambda < \Lambda_{\text{orb}}$. For $\Lambda = \Lambda_{\text{orb}}$, V_{eff} has a horizontal point of inflection at r_{orb}. From $V'_{\text{eff}}(r_{\text{orb}}) = 0$ and $V''_{\text{eff}}(r_{\text{orb}}) = 0$ we get

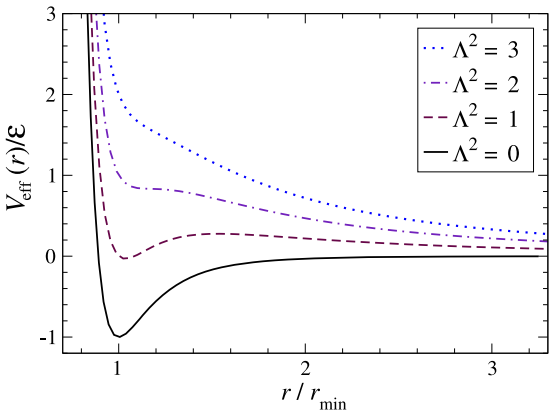

Fig. 1.7 Effective potential (1.33) for four values of Λ^2

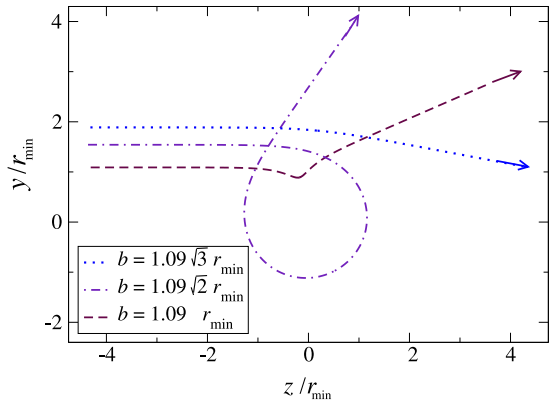

Fig. 1.8 Trajectories of a particle scattered by the Lennard–Jones potential (1.32) at energy $E = \mathscr{E}/(1.09)^2 \approx 0.84\mathscr{E}$. The three impact parameters correspond to $\Lambda^2 = 1$, $\Lambda^2 = 2$ and $\Lambda^2 = 3$, for which the effective potential is shown in Fig. 1.7

$$\begin{aligned} \frac{r_{\rm orb}}{r_{\rm min}} &= \left(\frac{5}{2}\right)^{1/6} \approx 1.165, \\ \Lambda^2_{\rm orb} &= \frac{18}{5}\left(\frac{2}{5}\right)^{2/3} \approx 1.954 \quad \text{and} \quad \frac{V_{\rm eff}(r_{\rm orb})}{\mathscr{E}} = \frac{4}{5}. \end{aligned} \tag{1.34}$$

If $E < \frac{4}{5}\mathscr{E}$, there will be an appropriate angular momentum $\Lambda < \Lambda_{\rm orb}$ for which the maximum of $V_{\rm eff}$, i.e. the top of the centrifugal barrier, coincides with E, so the conditions for orbiting are fulfilled. For $E = \frac{4}{5}\mathscr{E}$, orbiting occurs for $\Lambda = \Lambda_{\rm orb}$. If $E > \frac{4}{5}\mathscr{E}$, there is no orbiting.

Scattering trajectories are shown in Fig. 1.8 at energy $E/\mathscr{E} = 1/(1.09)^2 \approx 0.84$, which is just above the energy for which orbiting is possible. The impact parameters $b = r_{\rm min}\Lambda\sqrt{\mathscr{E}/E}$ correspond to $\Lambda^2 = 1, 2$ and 3 as featured in Fig. 1.7. In the closest collision ($\Lambda^2 = 1$), the particle passes above the centrifugal barrier associated with the attractive $-1/r^6$ potential tail, but instead of crashing into the origin it is reflected off the repulsive $1/r^{12}$ core at short distances. For the largest impact parameter ($\Lambda^2 = 3$), the radial motion is reflected by the centrifugal barrier, and the

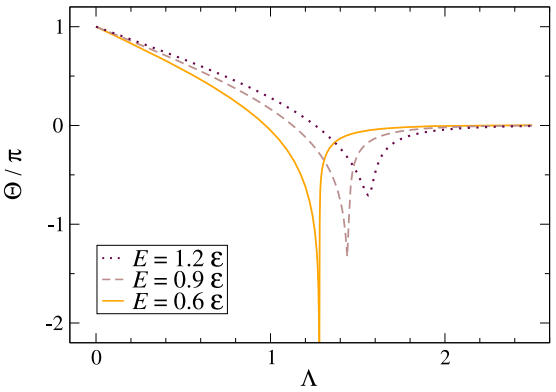

Fig. 1.9 Deflection function for scattering by the Lennard–Jones potential (1.32) for three energies. The abscissa is labelled by $\Lambda = \sqrt{E/\mathscr{E}}\, b/r_{\min}$

particle only weakly feels the attractive tail of the potential. The case in between, $\Lambda^2 = 2$, is close to the orbiting situation and the particle almost fulfills a complete revolution before leaving the interaction region.

Deflection functions for the Lennard–Jones potential (1.32) are shown in Fig. 1.9 for three energies. For $E/\mathscr{E} = 0.6$, orbiting occurs at $\Lambda \approx 1.281$. For $E/\mathscr{E} = 0.9$ and 1.2, orbiting is no longer possible, but pronounced minima of Θ with gradually decreasing depths remain.

1.3 Scattering Angle and Scattering Cross Sections

A typical scattering experiment involves a beam of incoming particles with uniform density n and asymptotic incoming velocity $\mathbf{v}_\infty = v_\infty \mathbf{e}_z$. The scattered particles are observed with a detector under an angle θ relative to the direction of incidence, see Fig. 1.10. The *scattering angle* θ varies between zero (forward scattering) and π (backward scattering).

The differential $\mathrm{d}\sigma$ is a quantitative measure for the flux of particles scattered into a differential solid angle $\mathrm{d}\Omega = \sin\theta\, \mathrm{d}\theta\, \mathrm{d}\phi$. It is defined as the number of particles passing a given (large) distance from the scattering centre in the direction of $\mathrm{d}\Omega$ per unit time, divided by the magnitude of the incoming current density, $|\mathbf{j}_{\mathrm{in}}| = n v_\infty$. If particles incident with impact parameter b are scattered into the angle θ, then, the particles scattered into the differential solid angle $\mathrm{d}\Omega$ are those with incoming trajectories passing through the differential area $\mathrm{d}b \times b\, \mathrm{d}\phi$ as shown in Fig. 1.10. The number of particles scattered into $\mathrm{d}\Omega$ per unit time is $n v_\infty \times b\, \mathrm{d}b\, \mathrm{d}\phi$, so

$$\mathrm{d}\sigma = b\, \mathrm{d}b\, \mathrm{d}\phi = b \left| \frac{\mathrm{d}b}{\mathrm{d}\theta} \right| \mathrm{d}\theta\, \mathrm{d}\phi = \frac{b}{\sin\theta} \left| \frac{\mathrm{d}b}{\mathrm{d}\theta} \right| \mathrm{d}\Omega . \tag{1.35}$$

The expressions in (1.35) contain the absolute value of $\mathrm{d}b/\mathrm{d}\theta$, because the observed yield is positive, regardless of whether $\mathrm{d}b/\mathrm{d}\theta$ is positive or negative.

The scattering angle $\theta \in [0, \pi]$ must not be confused with the deflection function $\Theta(b)$ discussed in Sect. 1.2. Among the particles observed under the scattering angle θ, there are those with incoming trajectories above the z-axis, as shown

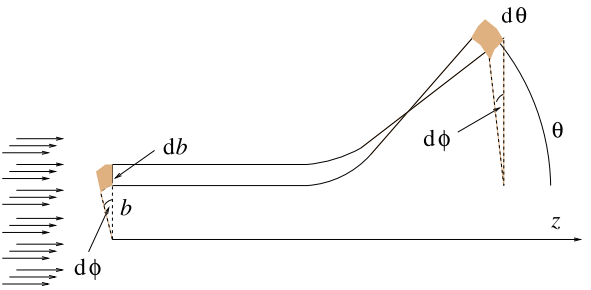

Fig. 1.10 Schematic illustration of a scattering experiment. Out of the uniform incoming beam, all trajectories with impact parameter between b and $b + \mathrm{d}b$ are observed with a scattering angle between θ and $\theta + \mathrm{d}\theta$

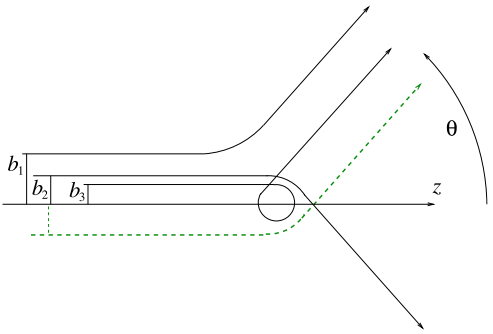

Fig. 1.11 Schematic illustration of different values of the deflection function corresponding to the same scattering angle θ: $\Theta(b_1) = \theta$, $\Theta(b_2) = -\theta$, $\Theta(b_3) = \theta - 2\pi$

in Fig. 1.10, for which $\Theta(b) = \theta$. However, there may also be particles with incoming trajectories below the z-axis, corresponding to a scattering plane rotated by π around the z-axis. An example is given by the dashed trajectory in Fig. 1.11 Such particles are detected under the scattering angle θ if $\Theta(b) = -\theta$. A scattering experiment in three dimensions usually does not discriminate between these two possibilities. Furthermore, one or more revolutions around the scattering centre are not detected, so observation under the scattering angle θ records all particles with impact parameter b for which $\pm(\Theta(b) + 2M\pi) = \theta$, i.e.,

$$\Theta(b) = \pm\theta - 2M\pi, \quad M = 0, 1, 2 \ldots . \tag{1.36}$$

The case $b = b_3$ in Fig. 1.11 is an example for $\Theta(b) = \theta - 2\pi$.

The *differential scattering cross section* as function of the scattering angle θ is obtained by summing the contributions (1.35) over all impact parameters fulfilling (1.36),

$$\frac{\mathrm{d}\sigma}{\mathrm{d}\Omega}(\theta) = \sum_i \frac{b_i}{\sin\theta}\left|\frac{\mathrm{d}b}{\mathrm{d}\theta}\right| = \sum_i \frac{b_i}{\sin\theta}\left[\left|\frac{\mathrm{d}\Theta}{\mathrm{d}b}\right|_{b_i}\right]^{-1}. \tag{1.37}$$

The area $\mathrm{d}\sigma$ corresponds to the area perpendicular to the incoming beam, through which all trajectories pass which are scattered into the solid angle $\mathrm{d}\Omega$. The expression on the far right of (1.37) is often preferred, because $\Theta(b)$ is an unambiguous function of the impact parameter b, defined on the interval $[0, \infty)$. In the preceeding expression, different terms in the sum correspond to different branches of the multivalued function $b(\theta)$.

The *integrated* or *total* scattering cross section σ is obtained by integrating the differential scattering cross section (1.37) over all angles of the unit sphere,

$$\sigma = \int \frac{\mathrm{d}\sigma}{\mathrm{d}\Omega}\mathrm{d}\Omega = 2\pi \int_0^\pi \frac{\mathrm{d}\sigma}{\mathrm{d}\Omega}(\theta)\sin\theta\,\mathrm{d}\theta. \tag{1.38}$$

The total scattering cross section corresponds to the area perpendicular to incidence through which all trajectories pass which are scattered at all.

For scattering by a hard sphere of radius R, the deflection function (1.9) is a bijective function of the impact parameter on the domain $b \in [0, R]$ where $\Theta = \theta$ and $b = R\cos(\theta/2)$, so

$$\frac{\mathrm{d}\sigma}{\mathrm{d}\Omega} = \frac{b}{\sin\theta}\left|\frac{\mathrm{d}b}{\mathrm{d}\theta}\right| = \frac{R^2}{4}. \tag{1.39}$$

Equation (1.39) shows that the hard sphere scatters isotropically. The total scattering cross section is, according to (1.38), simply 4π times the differential cross section (1.39), $\sigma = \pi R^2$, which is just the geometric cross section, i.e., the area of the obstacle as seen by the incident beam.

For a potential $V(r)$ which approaches zero smoothly as $r \to \infty$, the total scattering cross section is infinite, because even trajectories with very large impact parameters are scattered into small but nonvanishing scattering angles. For a potential falling off as $V(r) \sim C_\alpha/r^\alpha$ asymptotically, $\Theta(b) \propto 1/b^\alpha$ according to (1.19), and the differential scattering cross section (1.37) diverges in the forward direction as

$$\frac{\mathrm{d}\sigma}{\mathrm{d}\Omega}(\theta) \overset{\theta\to 0}{\sim} \frac{1}{\theta^{2+2/\alpha}}\frac{1}{\alpha}\left[\sqrt{\pi}\frac{|C_\alpha|}{E}\frac{\Gamma[(1+\alpha)/2]}{\Gamma(\alpha/2)}\right]^{2/\alpha}. \tag{1.40}$$

1.3.1 Kepler–Coulomb Potential

The Kepler–Coulomb potential $V(r) = C/r$ was introduced in Sect. 1.2.1, Eq. (1.20). The deflection function $\Theta(b)$ is given in (1.24) and shown in the right-hand part of Fig. 1.4. It is a bijective mapping of the interval $[0, \infty)$ onto a finite interval of deflection angles: $(0, \pi]$ in the repulsive case $C > 0$ and $[-\pi, 0)$ in the attractive case $C < 0$. The relation between scattering angle and deflection angle is $\theta = \Theta$ for $C > 0$ and $\theta = -\Theta$ for $C < 0$. Explicitly,

$$\begin{aligned} \Theta(b) &= \pm 2\arccos\left(\frac{1}{\sqrt{\gamma^2+1}}\right), \\ \gamma = \frac{|C|}{2Eb} &= \left|\tan\left(\frac{\theta}{2}\right)\right| \;\Rightarrow\; b = \left|\frac{C}{2E}\cot\left(\frac{\theta}{2}\right)\right|. \end{aligned} \tag{1.41}$$

The differential scattering cross section follows via (1.37),

$$\left|\frac{\mathrm{d}b}{\mathrm{d}\theta}\right| = \frac{|C|}{4E}\frac{1}{\sin^2(\theta/2)}, \quad \text{so} \quad \frac{\mathrm{d}\sigma}{\mathrm{d}\Omega} = \left(\frac{C}{4E}\right)^2 \frac{1}{\sin^4(\theta/2)} = \left(\frac{\mathrm{d}\sigma}{\mathrm{d}\Omega}\right)_{\text{Ruth}}, \tag{1.42}$$

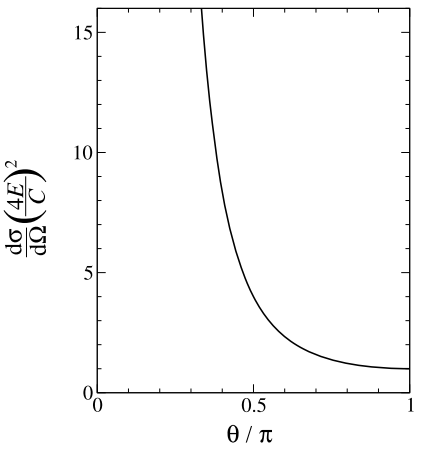

Fig. 1.12 Rutherford cross section (1.42) for scattering by the Kepler–Coulomb potential (1.20)

and it is shown in Fig. 1.12. This is the famous *Rutherford formula* for the differential cross section in Coulomb scattering. It does not discriminate between the repulsive case $C > 0$ and the attractive case $C < 0$.

1.3.2 Inverse-Power Potentials

Inverse-power potentials $V(r) = C_\alpha / r^\alpha$ were introduced in Sect. 1.2.2, Eq. (1.25). The deflection function is shown for the example $\alpha = 4$ in the right-hand part of Fig. 1.6. For the repulsive case, $C_\alpha > 0$, the deflection function $\Theta(b)$ is a bijective mapping of the interval $[0, \infty)$ onto $[0, \pi)$ and $\Theta = \theta$. The scattering cross section diverges in the forward direction according to (1.40) and is a monotonically decreasing function of the scattering angle. For an attractive inverse-power potential with $\alpha < 2$, there is no centrifugal barrier, and the scattering cross section is also a monotonically decreasing function of θ.

When $C_\alpha < 0$ and $\alpha > 2$, there is a centrifugal barrier and orbiting occurs when the parameter $\gamma = \alpha |C_\alpha| / (2Eb^\alpha)$ is equal to the value γ_{orb} given in Eq. (1.28), which, for given values of E and C_α, corresponds to the impact parameter

$$b_{\text{orb}} = \left(\frac{\alpha |C_\alpha|}{2E\gamma_{\text{orb}}} \right)^{1/\alpha} = \left(\frac{\alpha |C_\alpha|}{2E} \right)^{1/\alpha} \frac{\sqrt{\alpha}}{(\alpha - 2)^{(\alpha-2)/(2\alpha)}}. \tag{1.43}$$

As b increases from b_{orb} to infinity, $\Theta(b)$ grows from $-\infty$ to zero. For each scattering angle $\theta \in (0, \pi)$, there is an infinite sequence of impact parameters for which $\Theta + 2M\pi = \theta$ or $\Theta + 2M\pi = -\theta$. The derivative $|\mathrm{d}\Theta / \mathrm{d}b|$ is very large near orbiting, so the contribution of near-orbiting trajectories to the differential scattering cross section (1.37) is quite small. The small range of impact parameters near b_{orb} contributes rather uniformly to all scattering angles. The differential scattering cross section is shown in Fig. 1.13 for an inverse-power potential (1.25) with $\alpha = 4$.

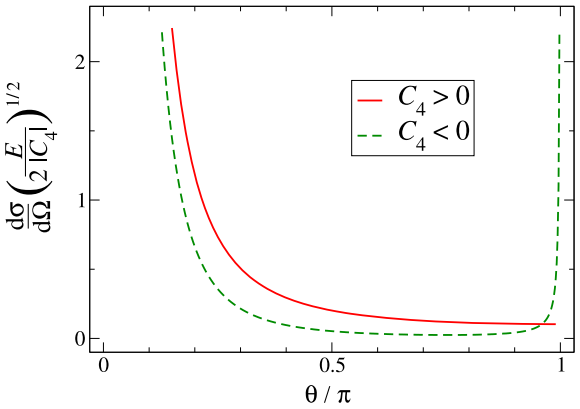

Fig. 1.13 Differential scattering cross section for an inverse-power potential (1.25) with $\alpha = 4$

Finite impact parameters for which $\Theta(b)$ is an odd multiple of π (corresponding to backward scattering) give a divergent contribution to the cross section due to the $\sin\theta$ in the denominator of the expression (1.37). Such divergent enhancement of the backward scattering cross section is referred to as *glory scattering*. The name stems from a similar effect in light scattering [1]. Note that the integration of the differential scattering cross section over a small finite range of angles near $\theta = \pi$ will lead to a finite result, because the diverging factor $1/\sin\theta$ in the cross section is compensated by the factor $\sin\theta$ in the differential $d\Omega$.

Glory scattering also occurs for finite impact parameters for which $\Theta(b)$ is an even multiple of π ("forward glory"). For potentials falling off smoothly to zero when $r \to \infty$, the effect of the forward glory is swamped by the generic forward divergence of the differential scattering cross section, see Eq. (1.40).

For an attractive inverse-power potential (1.25) with $\alpha > 2$, particles with impact parameters smaller than the orbiting value b_{orb} defined in (1.43) crash into the origin, where they may be absorbed by a variety of physical processes. The *absorption cross section* σ_{abs}, defined as the number of particles absorbed per unit time, divided by the incoming current density $n v_\infty$, is simply the area perpendicular to incidence through which the corresponding trajectories pass. Assuming that all particles incident with impact parameters $b < b_{\text{orb}}$ are absorbed yields

$$\sigma_{\text{abs}} = \pi b_{\text{orb}}^2 = \pi\alpha\left(\frac{|C_\alpha|}{2E}\right)^{2/\alpha}\left(\frac{1}{\alpha-2}\right)^{1-2/\alpha}. \tag{1.44}$$

For an inverse-square potential (1.30) with $C_2 < 0$, particles crash into the origin if $b \le \sqrt{|C_2|/E}$. If all these particles are absorbed,

$$\sigma_{\text{abs}} = \pi\frac{|C_2|}{E}, \tag{1.45}$$

which corresponds to the result (1.44) in the limit $\alpha \to 2$.

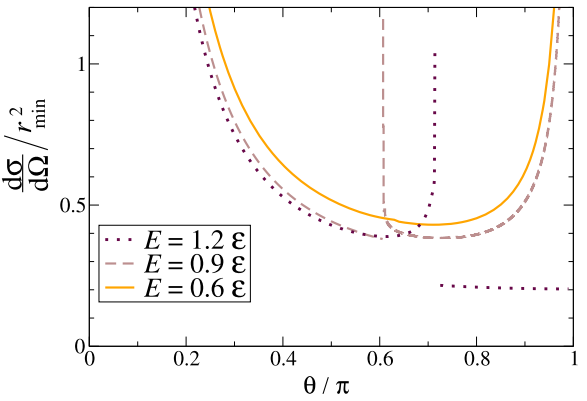

Fig. 1.14 Differential scattering cross section for the Lennard–Jones potential (1.32). For $E = 0.9\mathscr{E}$, there is a rainbow at $\theta_R \approx 0.61\pi$ and the dark side is towards smaller scattering angles. For $E = 1.2\mathscr{E}$, there is a rainbow at $\theta_R \approx 0.71\pi$ and the dark side is towards larger scattering angles

1.3.3 Lennard–Jones Potential

The Lennard–Jones potential (1.32) was discussed in Sect. 1.2.3, and deflection functions are shown in Fig. 1.9 for three energies. Differential scattering cross sections are shown in Fig. 1.14 for the same energies. At the lowest energy, $E = 0.6\mathscr{E}$, orbiting occurs and the behaviour of the cross section is qualitatively similar to that of the attractive $1/r^4$ potential shown in Fig. 1.13: there is divergence at backward angles corresponding to glory scattering, and the generic forward divergence. At $E = 0.9\mathscr{E}$, there is no orbiting, but the deflection function passes $-\pi$ for two finite values of the impact parameter, so glory scattering is still observable.

The deflection function at $E = 0.9\mathcal{E}$ has a minimum value $\Theta_{\min} \approx -1.39\pi$ for $\Lambda \approx 1.45$. At the corresponding scattering angle, $\theta_R = \Theta_{\min} + 2\pi \approx 0.61\pi$, the differential scattering cross section (1.37) diverges, because $\mathrm{d}\Theta/\mathrm{d}b$ vanishes. Such a divergence is called a *rainbow singularity*, because an analogous effect in light scattering is responsible for the rainbows in the sky [1]. The corresponding scattering angle θ_R is the *rainbow angle*. For $\theta > \theta_R \approx 0.61\pi$, there are five branches of $b(\theta)$ contributing to the scattering cross section (1.37), namely two with $\theta = \Theta + 2\pi$, two with $\theta = -\Theta$ and one with $\theta = \Theta$. The two branches with $\theta = \Theta + 2\pi$ coalesce at θ_R and no longer contribute for $\theta < \theta_R$, so only the three contributions with $\theta = \pm\Theta$ remain. For this rainbow, the regime $\theta < \theta_R$ is the *dark side* of the rainbow, while the regime $\theta > \theta_R$ is the *bright side* of the rainbow. The differential cross section (1.37) is noticeably smaller on the dark side of a rainbow than on the bright side.

At $E = 1.2\mathscr{E}$, the deflection function has a minimum $\Theta_{\min} \approx -0.71\pi$ at $\Lambda \approx 1.56$. The rainbow angle is now $\theta_R = -\Theta_{\min}$, and the dark side of the rainbow is $\theta > \theta_R$, while $\theta < \theta_R$ is the bright side. Note that $\Theta(b)$ never passes an odd multiple of π beyond $b = 0$, so there is no glory scattering at $E = 1.2\mathscr{E}$.

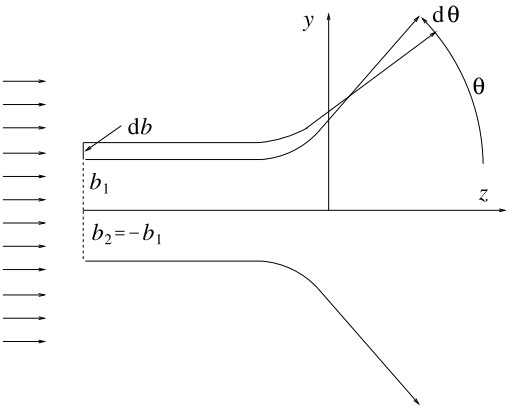

Fig. 1.15 Schematic illustration of a two-dimensional scattering experiment in the y–z plane. The impact parameter can be positive or negative (or zero), and the scattering angle θ varies between $-\pi$ and π

1.4 Classical Scattering in Two Spatial Dimensions

Two-dimensional scattering problems arise naturally when the motion of a particle is physically restricted to a plane. Furthermore, a three-dimensional scattering problem is effectively two-dimensional, if the physical system is translationally invariant in one direction, as is, e.g., the case for scattering of an atom by an infinitely long cylindrical wire.

As in three-dimensional scattering, we choose the z-axis to lie in the direction of incidence. The scattering potential is assumed to be radially symmetric, and the incoming particle with mass μ initially moves on a straight-line trajectory displaced by the impact parameter b from the z-axis. In three dimensions, this set-up is axially symmetric around the z-axis, and we chose the scattering plane to be the y–z plane with $b = L\sqrt{2\mu E} \geq 0$, see Fig. 1.1. In the 2D case, axial symmetry is replaced by reflection symmetry at the z-axis, and we could again choose the y–z plane such, that $b \geq 0$. We shall, however, adopt the more customary and convenient approach, where the y-z plane is assumed given by the physical system, so the impact parameter can be positive or negative (or zero), while the observable scattering angle θ varies between $-\pi$ and π—as sketched in Fig. 1.15.

For a given potential $V(r)$, the deflection function $\Theta(b)$ is the same as described in Sect. 1.2 for nonnegative b. Since the equations of motion are invariant under reflection at the z-axis, the deflection function for negative impact parameters follows via

$$\Theta(-b) = -\Theta(b), \tag{1.46}$$

i.e. the deflection function is an *antisymmetric* function of the impact parameter. When $\Theta(0) \neq 0$, i.e., $\lim_{b\to 0}\Theta(b) = m\pi$ with $m \neq 0$, then the deflection function shows a jump of $2m\pi$ at $b = 0$. As an example, Fig. 1.16 shows the deflection function for the Kepler–Coulomb potential $V(r) = C/r$, adapted to the two-dimensional case.

Particles scattered into a given scattering angle $\theta \in (0, \pi)$ are those with impact parameter b fulfilling (1.36). For each positive impact parameter b for which

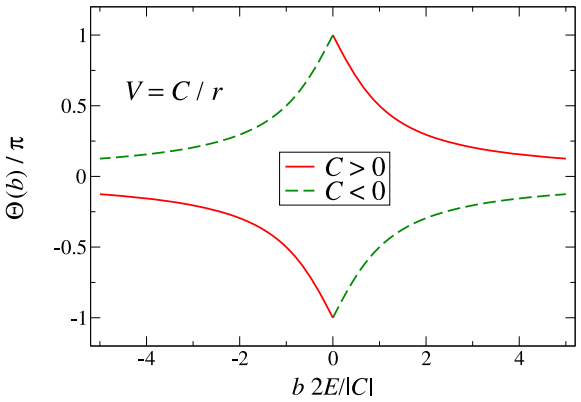

Fig. 1.16 Deflection function (1.24) for the Kepler–Coulomb potential, adapted to the two-dimensional case

$\Theta(b) = -\theta - 2M\pi$, the negative impact parameter $-b$ leads to the deflection angle $\Theta(-b) = \theta + 2M\pi$ because of (1.46). Trajectories of particles scattered into $-\theta$ are the reflections at the z-axis of those scattered into θ.

Adapting (1.36) to the two-dimensional case we formulate: A given scattering angle $\theta \in (-\pi, \pi)$ accommodates all particles with impact parameters $b \in (-\infty, \infty)$ for which

$$\Theta(b) = \theta - 2M\pi, \quad M = 0, \pm 1, \pm 2 \ldots . \tag{1.47}$$

Equation (1.8) in Sect. 1.2 can be generalized to accommodate negative angular momenta, for which $\theta(t)$ is a monotonically increasing function of time. One consequence is, that the integer M on the right-hand side of (1.47) can only be negative for negative impact parameters b, while it can only be positive for positive b, as already formulated in (1.36).

The differential $\mathrm{d}\lambda$ is a quantitative measure for the number of particles scattered into angles between θ and $\theta + \mathrm{d}\theta$ per unit time, normalized to the incoming current density $n\upsilon_\infty$. For each impact parameter fulfilling (1.47), these particles are those with incoming trajectories passing through the differential length $\mathrm{d}b$ as shown in Fig. 1.15. The number of particles scattered into $\mathrm{d}\theta$ per unit time is $n\upsilon_\infty \times \mathrm{d}b$, so

$$\mathrm{d}\lambda \equiv \mathrm{d}b = \left|\frac{\mathrm{d}b}{\mathrm{d}\theta}\right| \mathrm{d}\theta. \tag{1.48}$$

The *differential scattering cross section* as function of the scattering angle θ is obtained by summing the contributions (1.48) over all impact parameters fulfilling (1.47),

$$\frac{\mathrm{d}\lambda}{\mathrm{d}\theta} = \sum_i \left|\frac{\mathrm{d}b}{\mathrm{d}\theta}\right| = \sum_i \left[\left|\frac{\mathrm{d}\Theta}{\mathrm{d}b}\right|_{b_i}\right]^{-1}. \tag{1.49}$$

The length $\mathrm{d}\lambda$ corresponds to the length perpendicular to the incoming beam, through which all particles pass that are scattered into the angle $\mathrm{d}\theta$. From the symmetry with respect to reflection at the z-axis, it follows that the differential scattering cross section (1.49) is an even function of θ.

The *integrated* or *total* scattering cross section is obtained by integrating the differential cross section (1.49) over all scattering angles:

$$\lambda = \int_{-\pi}^{\pi} \frac{\mathrm{d}\lambda}{\mathrm{d}\theta} \mathrm{d}\theta. \tag{1.50}$$

It corresponds to the length perpendicular to the incoming beam, through which all particles pass that are scattered at all.

The formulae (1.49) and (1.50) for scattering cross sections in 2D differ from the corresponding formulae (1.37) and (1.38) in 3D in that they are missing the factor $b_i / \sin\theta$ coming from the definition of the solid angle. So, although the deflection function in 2D scattering is the same as in 3D—supplemented by Eq. (1.46) to accommodate negative impact parameters—the scattering cross sections for analogous systems in 2D and 3D do show differences.

Scattering by a hard sphere of radius R in 3D corresponds in 2D to the scattering by a hard disc of radius R, and Fig. 1.2 in Sect. 1.2 can be used as illustration in this case as well. The deflection function is given by (1.9) with (1.46), so $b = R\cos(\theta/2)$ and the differential cross section is, according to (1.49),

$$\frac{\mathrm{d}\lambda}{\mathrm{d}\theta} = \left|\frac{\mathrm{d}b}{\mathrm{d}\theta}\right| = \frac{R}{2}\left|\sin\left(\frac{\theta}{2}\right)\right|. \tag{1.51}$$

Note that scattering by a hard disc is, in contrast to scattering by a sphere, not isotropic. It is peaked at backward angles, $\theta \to \pm\pi$, and it vanishes towards forward angles $\theta \to 0$. The depletion at forward angles is easily understood considering that particles scattered into small angles hit the disc near the edge of its projection onto the line perpendicular to incidence, i.e. for b near $\pm R$. In 3D, a whole circle of impact parameters with b near R and azimuthal angles from zero to 2π contributes to scattering into small angles. The integrated cross section for scattering by the hard disc is

$$\lambda = \frac{R}{2}\int_{-\pi}^{\pi} \left|\sin\left(\frac{\theta}{2}\right)\right| \mathrm{d}\theta = 2R, \tag{1.52}$$

which is the geometric cross section, i.e., the length occupied by the disc in the path of the incident particles.

As in 3D scattering, the integrated cross section is infinite for a potential falling off smoothly as $r \to \infty$. For $V(r) \overset{r\to\infty}{\sim} C_\alpha / r^\alpha$, the deflection function behaves according to (1.19) and the differential scattering cross section (1.49) diverges in the forward direction as

$$\frac{\mathrm{d}\lambda}{\mathrm{d}\theta} \overset{\theta\to 0}{\sim} \frac{1}{|\theta|^{1+1/\alpha}} \frac{1}{\alpha}\left[\sqrt{\pi}\frac{|C_\alpha|}{E}\frac{\Gamma[(1+\alpha)/2]}{\Gamma(\alpha/2)}\right]^{1/\alpha}. \tag{1.53}$$

Comparing the forward divergence in 2D (1.53) and 3D (1.40) gives the appealingly simple result,

$$\left[\frac{\mathrm{d}\lambda}{\mathrm{d}\theta}(\theta)\right]_{\mathrm{2D}} \overset{\theta\to 0}{\sim} \sqrt{\frac{1}{\alpha}\left[\frac{\mathrm{d}\sigma}{\mathrm{d}\Omega}(|\theta|)\right]_{\mathrm{3D}}}. \tag{1.54}$$

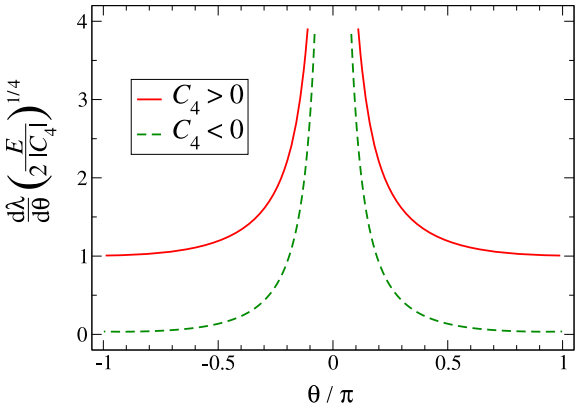

Fig. 1.17 Differential scattering cross section in two dimensions for an inverse-power potential (1.25) with $\alpha = 4$

For the Kepler–Coulomb potential $V(r) = C/r$, the deflection function is given analytically in (1.24) and displayed for the 2D situation in Fig. 1.16. The differential scattering cross section in 2D follows immediately via (1.49),

$$\frac{d\lambda}{d\theta} = \frac{|C|}{4E} \frac{1}{\sin^2(\theta/2)}. \tag{1.55}$$

In this case, the relation (1.54), with $\alpha = 1$, is not only valid asymptotically for $\theta \to 0$; it is an equality for all scattering angles.

The cross sections for the other examples discussed in Sect. 1.3 can also be derived via (1.49) using the deflection functions given in Sect. 1.2. Apart from the slower divergence at forward angles, a main difference is the absence of the glory singularity, which is due to the factor $1/\sin\theta$ in the 3D case. A main manifestation of orbiting and near-orbiting situations in 3D scattering, namely glory scattering at backward angles, is thus missing in the 2D cross sections. Figure 1.17 shows the differential scattering cross section (1.49) for an inverse-power potential $V(r) = C_4/r^4$. The ordinate is labelled with the cross section in units of the length $(2|C_4|/E)^{1/4}$.

For scattering by an attractive inverse-power potential $V(r) = C_\alpha/r^\alpha$, with $\alpha > 2$, orbiting occurs for impact parameters $|b| = b_{\rm orb}$, with $b_{\rm orb}$ given by (1.43). Assuming that all particles with impact parameters $|b| < b_{\rm orb}$ are absorbed, the absorbtion cross section is

$$\lambda_{\rm abs} = 2b_{\rm orb}. \tag{1.56}$$

The differential cross section for scattering by the Lennard–Jones potential (1.32) in two dimensions follows via (1.49)—and (1.46)—from the deflection functions discussed in Sect. 1.3.3, see Fig. 1.9. They are shown in Fig. 1.18 for the same energies as in Fig. 1.9 and Sect. 1.3.3. The rainbow singularities for $E = 0.9\mathscr{E}$ (at $\theta_{\rm R} \approx 0.61\pi$) and for $E = 1.2\mathscr{E}$ (at $\theta_{\rm R} \approx 0.71\pi$) are manifest, as in the 3D case.

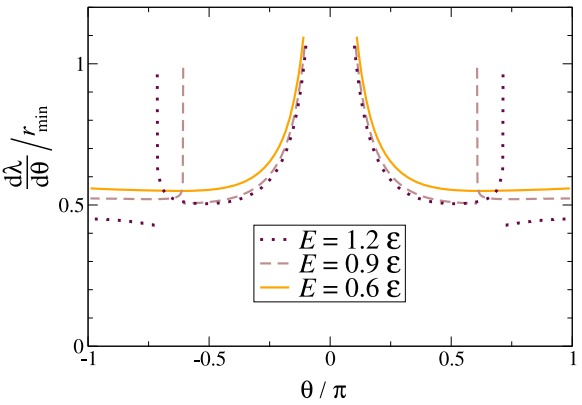

Fig. 1.18 Differential scattering cross section in two dimensions for the Lennard–Jones potential (1.32). For $E = 0.9\mathscr{E}$, there are rainbows at $|\theta| = \theta_R \approx 0.61\pi$ and the dark sides are towards smaller values of $|\theta|$. For $E = 1.2\mathscr{E}$, there are rainbows at $|\theta| = \theta_R \approx 0.71\pi$ and the dark sides are towards larger values of $|\theta|$

References

1. Adam, J.A.: The mathematical physics of rainbows and glories. Phys. Rep. **356**, 229–365 (2002)
2. Landau, L.D., Lifshitz, E.M.: Course of Theoretical Physics. Mechanics, vol. 1. 3rd edn. Butterworth-Heinemann, Stoneham (1976)